PROCEEDINGS OF SCIENCE

Polarized radio emission and radio wavefront shape of extensive air showers

A. Corstanje[*1], **S. Buitink**[3], , **J. E. Enriquez**[1], **H. Falcke**[1,4,5], **J. R. Hörandel**[1,4], **A. Nelles**[1,2], **J. P. Rachen**[1], **L. Rossetto**[1], **P. Schellart**[1], **O. Scholten**[6,7], **S. ter Veen**[1,5], **S. Thoudam**[1], **T. N. G. Trinh**[6]

1 *Department of Astrophysics/IMAPP, Radboud University Nijmegen, P.O. Box 9010, 6500 GL Nijmegen, The Netherlands*
2 *Now at: Department of Physics and Astronomy, University of California Irvine, Irvine, CA 92697-4575, USA*
3 *Astrophysical Institute, Vrije Universiteit Brussel, Pleinlaan 2, 1050 Brussels, Belgium*
4 *NIKHEF, Science Park Amsterdam, 1098 XG Amsterdam, The Netherlands*
5 *Netherlands Institute of Radio Astronomy (ASTRON), Postbus 2, 7990 AA Dwingeloo, The Netherlands*
6 *KVI-CART, University Groningen, P.O. Box 72, 9700 AB Groningen, The Netherlands*
7 *Interuniversity Institute for High-Energy, Vrije Universiteit Brussel, Pleinlaan 2, 1050 Brussels, Belgium*
E-mail: a.corstanje@astro.ru.nl

The LOFAR radio telescope located in the north of the Netherlands offers a high density of omnidirectional radio antennas. The LOFAR key science project Cosmic Rays is therefore well suited for detailed studies of the radio signal from air showers, and has been measuring since mid-2011 at primary energies in the range of 10^{17} to 10^{18} eV. We present high-precision measurements of the polarization of the radio signals, and the shape of the radio wavefront from the lateral distribution of signal arrival times. Polarization and timing of the incoming radio pulse are complementary observables to the lateral distribution of signal power. These are shown to provide additional information on the air shower geometry and on the contribution of different radio emission mechanisms, such as the geomagnetic and charge excess processes.

The 34th International Cosmic Ray Conference,
30 July- 6 August, 2015
The Hague, The Netherlands

[*]Speaker.

PoS(ICRC2015)396

1. Introduction

We use the LOFAR radio telescope [1] to measure radio emission from air showers. This radio signal reaches the antennas on the ground as a short pulse, with a duration on the order of 10 to 100 ns.

By timing the arrival of the pulses at each antenna, we measure the shape of the incident wavefront for individual air showers [2]. The wavefront is not planar, as most of the radio emission is produced at an altitude of a few kilometers. Geometry suggests that the amount of curvature depends on the height of the emission region and therefore on the depth of shower maximum, X_{max}.

The radio emission is strongly polarized, and the polarization is measured at individual antennas [3]. This gives insight in the contributions of different radio emission mechanisms [4] [5], most notably the geomagnetic [6] and charge-excess [7] mechanisms.

LOFAR is an array containing two types of antennas: the low-band antennas (LBA) sensitive to frequencies in a bandwidth of $10-90$ MHz, and the high-band antennas (HBA) operating in the $110-240$ MHz range. Air showers have been measured in both frequency ranges [8] [9]; these studies only use data from the LBAs. The bandwidth has been limited to $30-80$ MHz to reduce radio frequency interference. LOFAR is equipped with ring buffers (Transient Buffer Boards) that store the raw-voltage signals of each antenna for up to 5 seconds. These are used for air shower observations as described in [8].

Inside the inner core of LOFAR, which is a circular area of 320 m diameter, an array of 20 scintillator detectors (LORA) has been set up [10], which is used to trigger readout of the buffer boards once an air shower is detected. This yields a raw voltage time series for every antenna in a LOFAR station (a group of typically 96 LBA plus 48 HBA antennas), in which we identify and analyze the radio pulse from an air shower. Analysis of the particle detections delivers basic air shower parameters such as the estimated position of the shower axis, energy, and arrival direction.

The high density of antennas of LOFAR, together with a high timing resolution (200 MHz sampling rate) are especially favorable for measuring wavefront shapes and lateral distributions of the polarization.

2. Measurements of the radio wavefront shape

For this analysis we have used 165 air shower measurements with LOFAR. These consist of 2 milliseconds of raw voltage time series for every antenna of the LOFAR core stations; we have identified the radio pulse of the air shower in every individual trace, and measured its strength and arrival time. All measured air showers have been processed by the standard cosmic-ray reconstruction software as described in [8].

The arrival time of the radio pulse in each dipole is determined using the raw-voltage traces. We define the arrival time as the time of the pulse maximum in the amplitude of the analytic signal, also called Hilbert envelope. Using upsampling by a factor 32, this allows for arrival time measurements at a much higher time resolution the 5 ns sampling period of LOFAR. The attainable timing precision was found to be inversely proportional to signal-to-noise ratio (SNR), reaching 1 ns for an SNR of 12.7. We use this relation to define our timing uncertainties.

2.1 Shower-plane projection

We infer the general direction of the incoming pulse by obtaining the best-fitting plane wave solution to the arrival times of the radio pulse. This gives a first estimate of the direction of the shower axis. For the shower core position, where the shower axis reaches the ground, we employ the parametrization of the lateral distribution of signal power, from [11]. This gives an estimate of the core position to about 15 m accuracy.

Given the shower axis position and direction, we make a one-dimensional plot of the wavefront as a function of the distance to the shower axis. This assumes axial symmetry of the wavefront. In order to do this, all antenna positions are projected onto the shower plane, defined by the shower axis as its normal vector. A one-dimensional function describing the wavefront curvature can then be fitted to the arrival times as a function of distance to the shower axis.

The shower-plane projection is an approximation assuming that the angle between the curved wavefront and the shower plane is small. This is justified as the angles are on the order of 1 degree. For very large (extending to more than 1 km from shower core), or inclined air showers, a two-dimensional fitting procedure would be favored.

2.2 Fitting the wavefront shape

Various wavefront shapes have been proposed in the past; we have tested a conical and spherical shape [12], and a hyperboloid [2] [13], which combines curvature with a straight asymptote.

The fit function, for the arrival time differences with respect to a plane wave as a function of distance to the shower axis, is given for a hyperboloid as:

$$c\,t_{\mathrm{hyp}}(r) = -a + \sqrt{a^2 + b^2\,r^2}, \tag{2.1}$$

where a and b are the parameters of the hyperboloid.

This function is fitted using a non-linear least squares approach; the two parameters of the arrival direction are kept as free parameters in the fitting procedure, using a nested fitting to ensure that the optimum is reached.

2.3 Wavefront shape

The best-fitting shape was found to be a hyperboloid, as shown for an example air shower in Fig. 1. This holds for the entire data collection of 165 air showers that we have analyzed; a likelihood test has been done in order to ensure that the result is significant, even when taking into account that the hyperboloid has an extra free parameter compared to a cone or sphere (see [2]).

There is no significant sub-structure left in the fit residuals, hence we conclude that to our measurement accuracy, a hyperbolic parametrization is sufficient.

2.4 Correlations with air-shower parameters

We have evaluated how the steepness of the wavefront correlates with zenith angle. As a measure we have chosen the time lag at $r = 100$ m with respect to arrival at the shower axis, $r = 0$. It is not possible to use the hyperbola parameter b (the slope of the asymptote) directly, as for some air showers the asymptotic regime is far outside the data range.

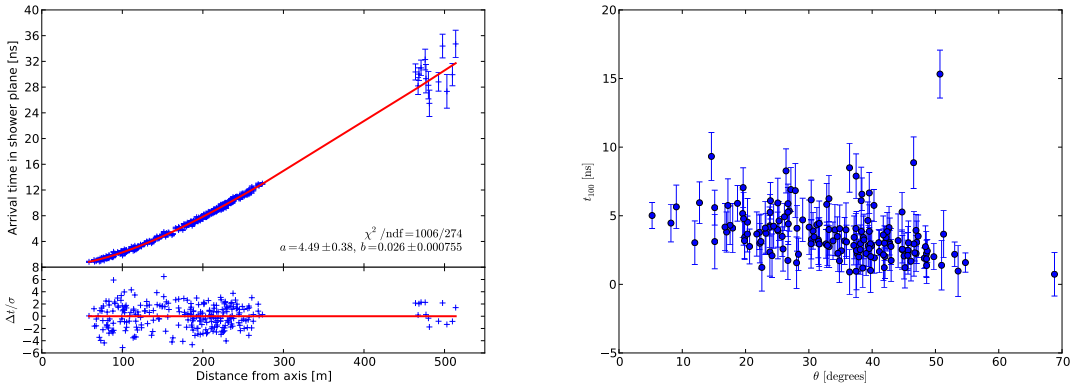

Figure 1: Left: An example measured wavefront from arrival times per antenna, showing the best-fitting hyperboloid, and in the lower panel the fit residuals. Right: dependence of wavefront steepness on zenith angle of the incoming air shower. The time lag at 100 m from the shower axis has been taken as a measure of wavefront steepness.

The right panel of Fig. 1 shows the time lag at 100 m as a function of zenith angle. There is a correlation, with a correlation coefficient of -0.32. The probability of obtaining this value for uncorrelated data is $4 \cdot 10^{-5}$, hence it is significant.

The angular deviation between wavefront and shower plane at 100 m distance on average amounts to 0.63 degrees, steepening to 0.94 degrees at 250 m. This agrees qualitatively with the value of 0.83 degrees found for a conical wavefront in [12]. As the angle is less than one degree, indeed precise timing is required in order to measure the wavefront shapes.

3. Polarization measurements

For the same set of air showers, we have analyzed the polarization in each individual antenna, fitting theoretical predictions of polarizations of the geomagnetic and charge-excess emission mechanisms.

3.1 Reconstructing polarized radio emission

For each antenna, we have combined the time traces of both polarizations, correcting for their complex gain [8]. These gains are obtained from antenna simulations and are calculated for a plane wave, arriving from direction $-\hat{\mathbf{e}}_v$, where $\vec{v}$ is the propagation velocity vector of the air shower, and polarized along $\hat{\mathbf{e}}_\theta$ or $\hat{\mathbf{e}}_\phi$. The resulting combined signals are then projected onto the $\hat{\mathbf{e}}_{\vec{v}\times\vec{B}}$ and $\hat{\mathbf{e}}_{\vec{v}\times\vec{v}\times\vec{B}}$ directions, with $\vec{B}$ the geomagnetic field vector. All antenna positions are projected onto the shower plane; the geometry is depicted in Fig. 2.

The arrival direction is the average of those obtained per station in a plane-wave fit. This has an estimated statistical uncertainty of $\sim 1^\circ$. Fitting a hyperbolic wavefront is not needed for the polarization analysis.

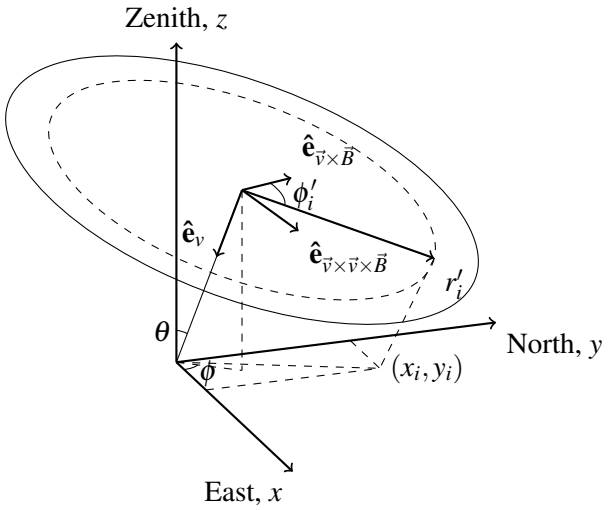

Figure 2: Geometry of the shower plane, defined by its normal vector $\hat{\mathbf{e}}_v$. All antenna positions (x_i, y_i) are projected onto this plane giving r_i, the distance to the shower axis and ϕ', the angle with the $\hat{\mathbf{e}}_{\vec{v}\times\vec{B}}$ direction. Note that the direction of $\hat{\mathbf{e}}_{\vec{v}\times\vec{B}}$ in this figure was chosen for clarity and does not reflect the direction of the magnetic field at LOFAR.

4. Determining the contributions of the emission mechanisms

Following [14] the expected electric field at any given time t can be written as

$$\begin{aligned}\vec{E}(t) &= \vec{E}_{\mathrm{G}}(t) + \vec{E}_{\mathrm{C}}(t) \\ &= (|\vec{E}_{\mathrm{G}}(t)| + |\vec{E}_{\mathrm{C}}(t)|\cos\phi')\hat{\mathbf{e}}_{\vec{v}\times\vec{B}} + \\ &\quad (|\vec{E}_{\mathrm{C}}(t)|\sin\phi')\hat{\mathbf{e}}_{\vec{v}\times\vec{v}\times\vec{B}}.\end{aligned} \tag{4.1}$$

Here $\vec{E}_{\mathrm{G}}(t)$ is the electric field produced by the geomagnetic contribution that is purely polarized along the direction of the Lorentz force, and $\vec{E}_{\mathrm{C}}(t)$ the radial electric field, produced by charge-excess. The charge-excess fraction is then defined as

$$a \equiv \sin\alpha \frac{|E_{\mathrm{C}}|}{|E_{\mathrm{G}}|}, \tag{4.2}$$

where $|E_{\mathrm{C}}|$ is the amplitude of the electric field produced by charge-excess when the total electric field vector amplitude reaches its maximum value.

The $\sin\alpha$ factor, with α the angle between the magnetic field $\vec{B}$ and the propagation direction of the shower $\vec{v}$, reflects the known dependence of the geomagnetic contribution. The charge-excess fraction, a, is determined from data by combining the equations for $\vec{E}$ and a, and fitting the resulting polarization angles given the parameter a. For details, see [3].

4.1 Polarization results

Since we expect the air shower signal to be completely polarized, the degree of polarization should be close to unity. Indeed, the measured degree of polarization has a median of 98.9%, and deviations from unity are caused by the unpolarized background noise.

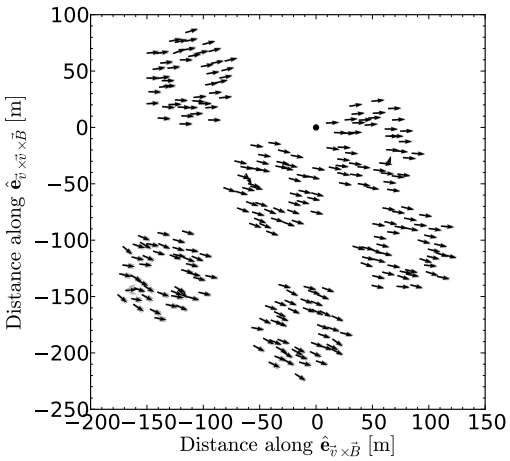

Figure 3: Polarization footprint of a single air shower as recorded with LOFAR, projected onto the shower plane. Each arrow represents the electric field measured by one antenna. The direction of the arrow is defined by the polarization angle; its length depicts the degree of polarization. The shower axis is indicated by the black dot at the origin. The median uncertainty on the angle of polarization is 4°.

The lateral distribution of the polarization, or polarization footprint, is depicted in Fig. 3 for an example air shower. Here, the angle and degree of polarization are depicted as arrows for each antenna position projected in the shower plane. As expected for geomagnetically dominated emission, the arrows are mostly aligned along the $\hat{\mathbf{e}}_{\vec{v}\times\vec{B}}$ direction. However, small deviations from this direction are visible. Deviations are interpreted to arise from the charge-excess component of the emission, introducing a component radially outward from the shower core.

4.2 Measurement of the radially polarized emission component

In the presence of a radially polarized emission component, with strength $a/\sin\alpha$ relative to the geomagnetic component, the angle of polarization depends on the observer location in the shower plane according to Eqs. (4.1), (4.2).

The charge-excess fraction can be fitted from the polarization data per air shower, given the equations above. These fits give an average charge-excess fraction of $(11 \pm 4)\%$ for our sample, where the uncertainty reflects the spread of the distribution. This measured presence of a radially polarized emission component is consistent with that produced by the charge-excess mechanism.

4.3 Dependence on shower arrival direction and radial distance to the shower axis

As explained in [15], the relative contributions of the charge-excess and geomagnetic components vary with opening angle from the emission maximum. We expect the charge excess fraction to increase towards larger distance from the shower axis. Also, at larger zenith angles, most of the emission is generated further away from the observer, and opening angles are therefore smaller. Thus, the charge-excess fraction decreases with increasing zenith angle.

To verify this, the measured charge excess fractions, as found by fitting the parameter a for all showers, have been combined. They have been grouped into bins of 50 m in radial distance, and of 20° in zenith angle.

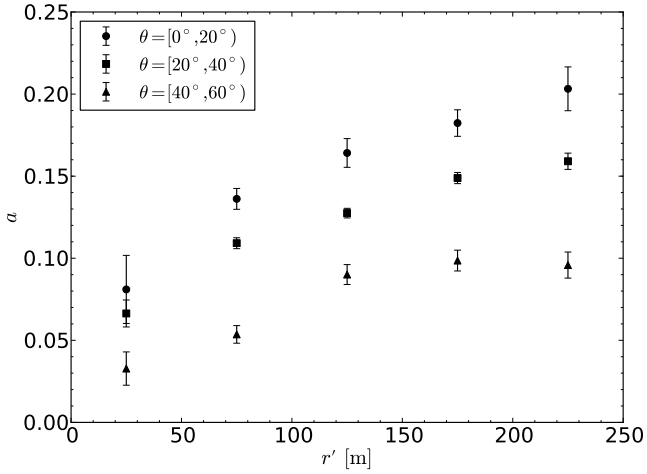

Figure 4: Charge-excess fraction (Eq. (4.2)) as a function of distance from the shower axis for three different zenith angle bins.

The result is shown in Fig. 4. For a description of the uncertainty calculation, see [3]. The predicted variations with radial distance and zenith angle are clearly seen. Quantitatively, the values are specific for this set of air showers, due to shower-to-shower fluctuations, and for the location of LOFAR (altitude, magnetic field).

5. Conclusions

Through pulse arrival timing, we have measured the radio wavefront shape of extensive air showers with LOFAR, to a precision of 1 ns per antenna. The best-fitting curve was found to be a hyperboloid, i.e. curved near the shower axis, and conical at large distances. This curve, with two free parameters, was also found to be sufficient to our measurement precision, as the fit residuals show no remaining structure.

We have analyzed the polarization of the radio pulses at each individual antenna. The polarization pattern is well described by a dominant geomagnetic contribution, parallel to the $\hat{\mathbf{e}}_{\vec{v}\times\vec{B}}$-direction, and a charge-excess contribution, with polarization radially outward from the shower core. Variations of the charge-excess fraction with distance to the shower axis and with zenith angle were found to be in agreement with theoretical predictions, although the absolute scale depends on the specific set of air showers that was used.

6. Acknowledgements

The LOFAR cosmic ray key science project acknowledges funding from an Advanced Grant of the European Research Council (FP/2007-2013) / ERC Grant Agreement n. 227610. The project has also received funding from the European Research Council (ERC) under the European Union's Horizon 2020 research and innovation programme (grant agreement No 640130). We furthermore acknowledge financial support from FOM, (FOM-project 12PR304) and NWO (VENI grant 639-041-130). AN is supported by the DFG (research fellowship NE 2031/1-1).

LOFAR, the Low Frequency Array designed and constructed by ASTRON, has facilities in several countries, that are owned by various parties (each with their own funding sources), and that are collectively operated by the International LOFAR Telescope foundation under a joint scientific policy.

References

[1] M. P. van Haarlem et al., *LOFAR: The LOw-Frequency ARray*, *Astronomy & Astrophysics* **556** (Aug., 2013) A2, [arXiv:1305.3550].

[2] A. Corstanje, P. Schellart, et al., *The shape of the radio wavefront of extensive air showers as measured with LOFAR*, *Astroparticle Physics* **61** (Feb., 2015) 22–31, [arXiv:1404.3907].

[3] P. Schellart et al., *Polarized radio emission from extensive air showers measured with LOFAR*, *JCAP* **10** (Oct., 2014) 14, [arXiv:1406.1355].

[4] O. Scholten, K. Werner, and F. Rusydi, *A macroscopic description of coherent geo-magnetic radiation from cosmic-ray air showers*, *Astroparticle Physics* **29** (2008), no. 2 94 – 103.

[5] K. Werner and O. Scholten, *Macroscopic treatment of radio emission from cosmic ray air showers based on shower simulations*, *Astroparticle Physics* **29** (2008), no. 6 393 – 411.

[6] F. D. Kahn and I. Lerche, *Radiation from Cosmic Ray Air Showers*, *Royal Society of London Proceedings Series A* **289** (Jan., 1966) 206–213.

[7] G. A. Askaryan, *Excess Negative Charge of the Electron-Photon Shower and Coherent Radiation Originating from It. Radio Recording of Showers under the Ground and on the Moon*, *Journal of the Physical Society of Japan Supplement* **17** (1962) C257.

[8] P. Schellart, A. Nelles, et al., *Detecting cosmic rays with the LOFAR radio telescope*, *Astronomy & Astrophysics* **560** (Dec., 2013) A98, [arXiv:1311.1399].

[9] A. Nelles, P. Schellart, and the LOFAR collaboration, *Measuring a Cherenkov ring in the radio emission from air showers at 110-190 MHz with LOFAR*, *Astroparticle Physics* **65** (2015) 11–21, [arXiv:1411.6865].

[10] S. Thoudam et al., *Lora: A scintillator array for {LOFAR} to measure extensive air showers*, *Nuclear Instruments and Methods in Physics Research Section A: Accelerators, Spectrometers, Detectors and Associated Equipment* **767** (2014), no. 0 339 – 346.

[11] A. Nelles, S. Buitink, H. Falcke, J. R. Hörandel, T. Huege, and P. Schellart, *A parameterization for the radio emission of air showers as predicted by CoREAS simulations and applied to LOFAR measurements*, *Astroparticle Physics* **60** (Jan., 2015) 13–24, [arXiv:1402.2872].

[12] F. G. Schröder and et al. LOPES collaboration, *Investigation of the Radio Wavefront of Air Showers with LOPES and REAS3*, in *International Cosmic Ray Conference*, vol. 3 of *International Cosmic Ray Conference*, p. 64, 2011.

[13] W. Apel et al., *The wavefront of the radio signal emitted by cosmic ray air showers*, *Journal of Cosmology and Astroparticle Physics* **2014** (2014), no. 09 025.

[14] A. Aab et al., *Probing the radio emission from air showers with polarization measurements*, *Physical Review D* **89** (Mar., 2014) 052002.

[15] K. D. de Vries, O. Scholten, and K. Werner, *The air shower maximum probed by Cherenkov effects from radio emission*, *Astroparticle Physics* **45** (May, 2013) 23–27, [arXiv:1304.1321].